Journal of
Dementia and Alzheimer's Disease

MDPI

Systematic Review

Early Detection of Alzheimer's Disease via Amyloid Aggregates: A Systematic Review of Plasma Spectral Biomarkers and Machine Learning Approaches

Stella Hernández [1,*], Sonia M. Valladares-Rodríguez [2], Mercedes Novo [1] and Wajih Al-Soufi [1]

[1] Departamento de Química Física, Facultade de Ciencias, Campus Terra, Universidade de Santiago de Compostela, 27002 Lugo, Spain; m.novo@usc.es (M.N.); wajih.al-soufi@usc.es (W.A.-S.)
[2] Departamento de Electrónica e Computación, Escola Politécnica Superior de Enxeñaría, Campus Terra, Universidade de Santiago de Compostela, 27002 Lugo, Spain; sonia.valladares@usc.es
* Correspondence: stella.hernandez.faria@usc.es

Abstract

Background: Early diagnosis of Alzheimer's disease (AD) is constrained by invasive and costly tests. Aggregation of β-amyloid and the Aβ42/Aβ40 ratio in cerebrospinal fluid (CSF) and blood are key biomarkers. Fluorescent probes can report aggregate states, and artificial intelligence (AI) can extract subtle patterns from spectral and blood data. This review synthesizes how probes and AI can identify aggregates and assess the Aβ42/Aβ40 ratio in body fluids to facilitate earlier AD diagnosis. **Methods:** PRISMA-compliant searches were conducted in Scopus, PubMed, Web of Science, and IEEE Xplore. **Results:** Twenty-eight studies met inclusion criteria. Plasma Aβ42/Aβ40 was lower in PET-positive individuals by ∼7–18%, with higher performance for mass spectrometry (mean AUC ≈ 0.80) than immunoassays (AUC ≈ 0.71). CSF Aβ42/Aβ40 showed larger group differences (∼50% reductions in PET+) and stronger PET concordance, outperforming plasma. Fluorescent probes—including AN-SP and CRANAD-28—were sensitive to early aggregates and showed in vivo imaging potential, but evidence is largely preclinical or from small cohorts. AI/ML approaches frequently achieved within-study accuracies >90% (e.g., 94–100% in spectral tasks), yet external validation and head-to-head tests of *ratio alone* versus *ratio + AI* remain scarce. **Conclusions:** Plasma Aβ42/40—particularly by mass spectrometry—currently provides the most reproducible fluid approximation to amyloid PET (mean AUC ≈ 0.80). Fluorescent probes sensitively detect oligomeric Aβ species and show in vivo potential, but evidence remains largely preclinical or from small cohorts. AI/ML methods can extract additional signal from spectral and multivariate blood data, yet consistent *incremental* gains over optimized Aβ42/40 assays have not been demonstrated due to limited external validation and head-to-head comparisons.

Keywords: Alzheimer's disease; β-amyloid aggregates; plasma Aβ42/40; fluorescence-based probes; machine learning

Academic Editor: Hualou Liang

Received: 4 June 2025
Revised: 29 August 2025
Accepted: 22 September 2025
Published: 18 October 2025

Citation: Hernández, S.; Valladares-Rodríguez, S.M.; Novo, M.; Al-Soufi, W. Early Detection of Alzheimer's Disease via Amyloid Aggregates: A Systematic Review of Plasma Spectral Biomarkers and Machine Learning Approaches. *J. Dement. Alzheimer's Dis.* **2025**, *2*, 38. https://doi.org/10.3390/jdad2040038

1. Introduction

Alzheimer's disease (AD) is a progressive neurodegenerative disorder and the leading cause of dementia worldwide [1]. Despite extensive research efforts, its exact cause remains unclear, and no disease-modifying treatments are currently available. The "amyloid hypothesis", the most widely accepted explanation for AD, proposes that accumulation and aggregation of β-amyloid (Aβ) peptides initiate a cascade of neurotoxic oligomeric

assemblies, neuroinflammation, and synaptic alterations. Pathologically, AD is characterized by extracellular deposition of Aβ peptides, particularly the Aβ40 and Aβ42 isoforms, and the intracellular accumulation of neurofibrillary tangles composed of hyperphosphorylated tau [2–6]. These pathological hallmarks contribute to synaptic dysfunction, neuronal death, and chronic neuroinflammation, ultimately resulting in cognitive decline [6,7]. Over the past two decades, soluble Aβ oligomers (AβOs)—formed early in the aggregation process—have emerged as the principal neurotoxic species in AD, exhibiting disease-dependent accumulation in the brains of affected individuals and driving synaptic dysfunction and neurodegeneration [8–11]. Detecting these AβOs at the earliest stages could therefore enable timely diagnosis and therapeutic intervention.

Currently, CSF assays and positron emission tomography (PET) imaging are the main tools used to detect Aβ aggregates and assess amyloid burden in the brain. Although these techniques provide reliable assessments, they are invasive, expensive, and not widely accessible, limiting their use in early-stage screening and routine clinical practice.

In recent years, increasing attention has turned to blood-based biomarkers as a less invasive and more scalable alternative. In particular, plasma Aβ42/40 has shown a stronger correlation with amyloid PET imaging than absolute Aβ levels [12,13]. Several studies have demonstrated that a reduced Aβ42/40 in plasma is associated with a higher risk of developing dementia [1,12–22].

Among the various strategies for detecting Aβ aggregates, fluorescence-based methods offer unique advantages in terms of sensitivity, versatility, and potential for in situ and real-time analysis. Fluorescent probes can be designed to respond to different stages of amyloid aggregation by exhibiting changes in fluorescence intensity, emission wavelength, or lifetime [23]. These probes include environment-sensitive dyes such as Thioflavin T and Congo Red, solvatochromic fluorophores, molecular rotors, and aggregation-induced emission (AIE) fluorogens. Compared to standard immunoassay-based techniques like ELISA and SIMOA, which rely on antibodies, fluorescent probes often offer simpler assay design and direct optical readout. In contrast to PET tracers, fluorescence methods are more cost-effective and compatible with high-throughput or point-of-care platforms. These advantages make fluorescence spectroscopy a promising alternative for detecting early-stage amyloid aggregates, especially when integrated with advanced data analysis techniques. However, the interpretation of fluorescence emission spectra from amyloid-binding probes is often complicated by spectral overlap, background autofluorescence, and dynamic heterogeneity of aggregates. These challenges necessitate advanced computational approaches capable of resolving subtle patterns in complex data.

In particular, AI-based methods (machine learning and related approaches) have emerged as promising approaches to resolve subtle patterns in high-dimensional, noisy fluorescence data, improving identification and quantification of Aβ oligomers in biological fluids. Several studies demonstrate how AI techniques—such as Random Forest (RF), XGBoost, Principal Component Analysis (PCA), and Linear Discriminant Analysis (LDA)—have been effectively applied to multichannel fluorescence data and spectral decomposition for accurate classification of AD-related patterns, achieving classification accuracies exceeding 90% [24–26]. Moreover, AI approaches have been used to integrate multiple biomarker modalities, including Aβ42/40, improving diagnostic accuracy and enabling patient stratification [27–29].

Building on these considerations, this systematic review addresses the following primary research question:

> How can fluorescent probes and AI-based tools facilitate the early diagnosis of Alzheimer's disease by identifying β-amyloid aggregates and assessing the Aβ42/Aβ40 ratio in body fluids?

In addition, the review explores the following sub-questions:

1. How accurately can measurement of Aβ42/40 in plasma detect AD compared to PET imaging?
2. Biomarkers: What specific biomarkers have shown efficacy in the early detection of β-amyloid aggregates?
3. Which ML techniques have contributed to the detection of Aβ aggregates and biomarkers in early-stage AD?

2. Methods

To adequately address the research question and sub-questions, this systematic review was conducted in accordance with the fundamentals of the Preferred Reporting Items for Systematic Reviews and Meta-Analyses (PRISMA) methodology. The following steps outline the approach taken:

2.1. Search Strategy

A literature search was conducted in Scopus, PubMed, Web of Science, and IEEE Xplore. The search included studies published from January 2014 to December 2024. The queries were carefully designed to capture all relevant literature and included Boolean operators, synonyms, and Medical Subject Headings (MeSH) terms. To structure the search effectively, we categorized keywords into five thematic groups: (1) Technology: Keywords related to techniques and measurement methods, such as biomarker and fluorescence spectroscopy, were included; (2) Analysis: This category focused on analytical methodologies, including terms like machine learning, data science, and spectral analysis; (3) Field of research: Keywords pertaining to the biological context, such as protein measurements, amyloid aggregates, and Aβ42/40, were prioritized; (4) Zone: This group targeted the measurement medium, using terms such as plasma, blood, CSF; and (5) Exclusion terms: Irrelevant keywords, including terms such as nanoparticles, cancer, and tumor, were excluded to refine the scope of the search and ensure relevance to the research question.

Examples of search queries for PubMed database include:

(biomarker* OR spectroscop* OR fluorescen* OR "biosensor")
AND
("machine learning" OR "deep learning" OR "data science" OR "artificial intelligence" OR spectr* analys*)
AND
(amyloid* aggregate OR amyloid* plaques OR amyloid* fibril* OR "abeta42/abeta40" OR amyloid* autofluorescence OR "early diagnosis" OR "Alzheimer" OR "Aβ42/40")
AND
("blood" OR "plasma" OR "CSF" OR "biological sample" OR "serum" OR "cerebrospinal fluid")
NOT
(nanoparticl* OR "nanocluster" OR tumor* OR "cancer" OR "cholesterol")

The query was adapted for each database. Figure 1 shows how many papers were returned in each database. Only works published since 2014 were used, in some database this requirement was possible to add in the query, like Scopus, in others not, like IEEE Xplore. After obtaining all the results, the articles were uploaded to Zotero to proceed with the elimination of duplicates.

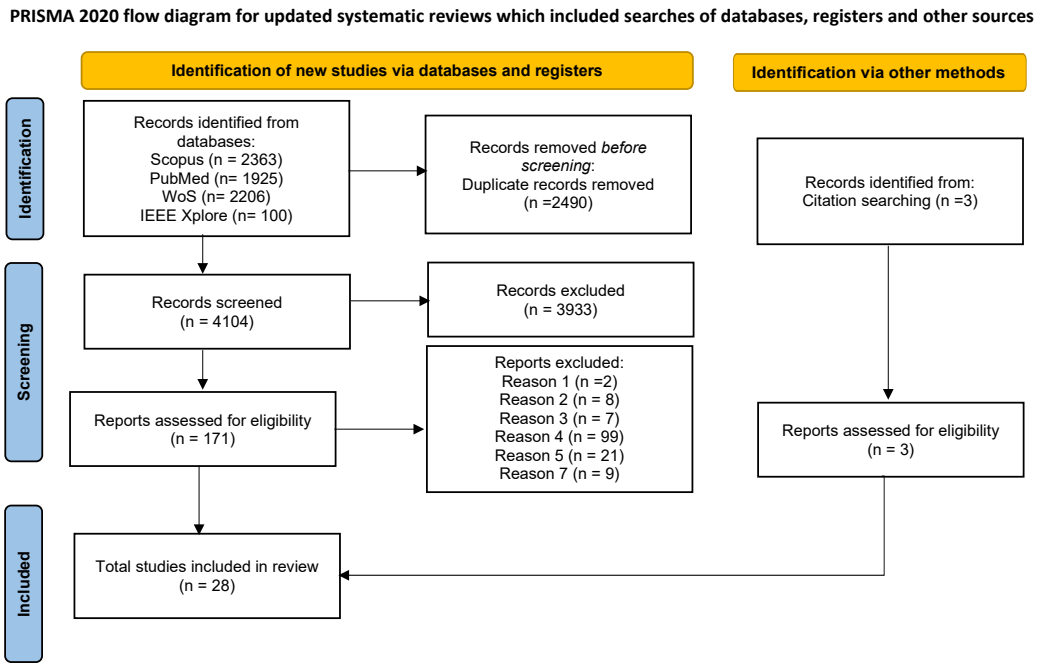

	Exclusion Criteria
	Population not focused on Alzheimer's disease or related neurodegenerative conditions.
	Studies that do not use plasma-based amyloid biomarkers or other biomarkers linked to amyloid aggregation.
	Studies that do not include spectral measurement techniques as part of the diagnostic evaluation.
	Non-peer-reviewed literature, editorials, opinion pieces, or studies with insufficient methodological transparency.
	Studies that are not articles, such as reviews or papers presented at conferences

Figure 1. PRISMA 2020 Flow Diagram for updated systematic review.

In an independent search, it was checked that the query used included all relevant publications. In this search, some adjustments were included: adding the term "oligomers", separating "amyloid" from "aggregate", "plaques", or "fibers", incorporating synonyms for "autofluorescence" such as "intrinsic fluorescence" or "endogenous fluorescence," and testing terms like "aggregat*" to capture all variations related to aggregation. To systematically assess the impact of these modifications, we developed a Python 3.12.0 program to compare the results obtained from the revised queries against our initial search. This program identified papers that appeared in the modified searches but were absent from our original dataset. After evaluating these additional papers, we found that none of them provided new relevant information for our bibliographic review, confirming the robustness of our initial search strategy.

This review did not include documents from patent repositories (e.g., WIPO, Espacenet) or clinical trial registries (e.g., ClinicalTrials.gov), as these sources often lack standardized methodological descriptions or validated results. In the context of this review, most entries in these databases do not specify the methodology or analytical techniques employed. Without this information, inclusion and comparison are not feasible, and these registries are outside the scope of our predefined inclusion criteria.

2.2. Eligibility Criteria

The following inclusion and exclusion criteria were followed to select the articles.

2.2.1. Inclusion Criteria

1. Research that investigates the relationship between amyloid aggregation and diagnostic outcomes for AD using Aβ42/40.
2. Studies focused on early diagnosis of AD using biomarkers for the Aβ aggregates, such as autofluorescence of the amyloid, or other plasma or CSF biomarkers.
3. Studies that provide quantitative data on biomarkers or other diagnostic tests associated with AD.
4. Studies that combine AI and ML with spectral measurements for analytic determination, regardless of whether the biomarker is directly related to amyloid.

2.2.2. Exclusion Criteria

1. Population not focused on AD or related neurodegenerative conditions.
2. Studies not addressing early diagnosis or studies that are focused on treatment clinical management, or late-stage disease.
3. Studies that do not use plasma-based amyloid biomarkers or other biomarkers linked to amyloid aggregation.
4. Studies that do not include spectroscopic techniques as part of the diagnostic evaluation.
5. Non-peer-reviewed literature, editorials, opinion pieces, or studies with insufficient methodological transparency.
6. Studies that do not apply AI or ML techniques for spectral data analysis or diagnostic purposes.
7. Studies that are not articles, such as reviews or papers presented at conferences.

We used Zotero functionalities to merge all references from all databases. After removal of all duplicate articles, a first screening was performed that reviewed the title, abstract, and keywords of each study to determine whether the study is relevant to the review based on the inclusion and exclusion criteria cited in this section. An initial screening was performed, checking the exclusion criteria. If there was some uncertainty, the study was flagged for further discussion. Studies that were not excluded at this first screening were moved on to the full text screening.

In the second stage of screening, the full text of all studies that passed the initial phase was reviewed. This stage also adhered to the established inclusion and exclusion criteria. If any study could not be clearly classified during the screening process, it was subjected to further evaluation by a senior reviewer. In the first screening phase, 171 papers were selected (Figure 1).

2.3. Diagnostic Evaluation Metrics

To support interpretation and comparison across methodologies, this review systematically analyzes key diagnostic performance metrics—such as sensitivity, specificity, accuracy, Spearman's correlation, and AUC—reported in the included studies. These indicators help evaluate the ability of fluorescence-based probes and AI-assisted analyses to detect early amyloid aggregation, distinguish AD from controls, and correlate with established biomarkers like Aβ42/40.

Accuracy: the proportion of correctly classified cases (both positive and negative) relative to the total number of cases. While widely used, accuracy can be misleading in data sets with imbalanced class distributions.

Sensitivity (true positive rate): Proportion of individuals with AD who are correctly identified as positive. High sensitivity ensures that most true cases are detected, reducing the likelihood of false negatives.

Specificity (true negative rate): Proportion of healthy individuals correctly identified as negative. High specificity minimizes false positives, which is important for avoiding undue anxiety or unnecessary interventions.

Spearman's rank correlation coefficient (ρ): A nonparametric measure used to assess the strength and direction of a monotonic relationship between two variables, such as between biomarker aggregation levels and Aβ42/40. Unlike Pearson's correlation, Spearman's ρ does not assume a linear relationship and is more robust to non-normally distributed data.

Receiver Operating Characteristic (ROC) Curve and Area Under the Curve (AUC): The ROC curve plots the true positive rate (sensitivity) against the false positive rate (1 − specificity) at various classification thresholds. The area under the ROC curve (AUC) provides a single-value measure of the discriminatory power of the model; an AUC of 1.0 indicates perfect classification, while an AUC of 0.5 suggests performance equivalent to random chance.

Centiloid: A standardized scale for PET imaging to quantify "global" cortical amyloid burden. The centiloid scale facilitates comparison across studies and tracers by transforming PET measures into a common metric [30].

3. Results

This systematic review aims to (i) summarize biomarkers for detecting amyloid aggregates, with emphasis on oligomers; (ii) evaluate the plasma and CSF Aβ42/40 for early AD detection; and (iii) assess how AI/ML methods and tools can enhance pre-diagnostic performance (AUC, sensitivity, specificity).

As illustrated in Figure 1, a total of 6594 papers were initially retrieved from the four selected databases. After eliminating 2490 duplicates, 4104 articles proceeded to the title and abstract screening, with 171 advancing to the second stage of screening.

Following this process, 25 studies were selected for inclusion in the final analysis. One example of an excluded study is "A Possible Blood Plasma Biomarker for Early-Stage Alzheimer's Disease" [31], the exclusion criterion applied in this case was criterion 4. Although the study addresses early detection of AD and involves a biomarker, it does not employ fluorescence techniques. The biomarker used is not a dye, and the detection method is based on mass spectrometry rather than optical fluorescence. Additionally, 3 external papers identified from the references of the final 25 studies were included, bringing the total number of studies considered to 28.

These studies were categorized into three main groups: (1) studies focused on comparing plasma Aβ42/40 between PET-positive (PET+) and PET-negative (PET-) individuals; (2) studies investigating fluorescent biomarkers for the detection of amyloid aggregates, including oligomers and fibers; (3) studies employing ML and AI techniques on databases of spectral data to enhance the diagnosis of AD. The relevant information extracted from the papers of each group is collected in Tables 1–3. Also, the cohorts used in each of the studies in Table 1 are collected in Table 4.

This classification enabled a structured analysis of the current landscape of biomarker-based detection methods and the potential of AI-driven tools to facilitate early diagnosis.

Table 1. Summary of papers with analysis of plasma Aβ42/40.

Reference	Study Title	Medium	Measurement Method	**Aβ42/40** (vs. PET)	AUC (95% CI)	Reference Standard	Notes
West et al. (2021) [22]	A blood-based diagnostic test incorporating plasma Aβ42/40 ratio, ApoE proteotype, and age accurately identifies brain amyloid status: findings from a multi-cohort validation	Plasma	Plasma Aβ quantification using LC-MS/MS	Plasma Aβ42/40 was significantly lower in amyloid-positive (PET+). Plasma Aβ42/40 was, on average, 11.4% lower in the amyloid-positive group than in the amyloid-negative group	Plasma Aβ42/40: 0.86	CSF and PET	False positives may reflect an earlier stage of amyloid pathology before PET scans can detect plaques
Gao et al. (2022) [15]	A combination model of AD biomarkers revealed by machine learning precisely predicts Alzheimer's dementia: China Aging and Neurodegenerative Initiative (CANDI) study	Plasma	Aβ40, Aβ42, phosphorylated tau (p-tau), and total tau (t-tau) were measured using the Single Molecule Array (Simoa) technology	Plasma Aβ42/40 was significantly lower in PET-positive (PET+) individuals	Plasma Aβ42/40 AUC (CI: 95%) for identifying brain amyloid positivity: AUC = 0.718 - Compare to PET AUC = 0.738 - Compare to CSF	CSF and PET	-
Udeh-Momoh et al. (2022) [14]	Blood derived amyloid biomarkers for Alzheimer's disease prevention	Plasma	Six different plasma Aβ42/40 measurement platforms were tested: Immunoassays (IA): Roche, Quanterix, ADx Neurosciences Mass spectrometry (MS): WashU, Shimadzu, Gothenburg	Plasma Aβ42/40 was 7–12% lower in PET+ individuals than in PET- individuals	Discriminative power for detecting PET amyloid positivity in cognitively unimpaired (CU) individuals: WashU (MS-based): AUC = 0.753 (0.601–0.905) ($p = 0.003$): Best performer Roche (IA-based): AUC = 0.737 (0.597–0.877) ($p = 0.006$): Second-best Shimadzu (MS-based): AUC = 0.695 (0.545–0.845) ($p = 0.023$) Quanterix (IA-based): AUC = 0.693 (0.540–0.847) ($p = 0.025$)	PET	WashU (MS) and Roche (IA) were the most effective assays, supporting their potential clinical utility
Pascual-Lucas et al. (2023) [13]	Clinical performance of an antibody-free assay for plasma Aβ42/40 to detect early alterations of Alzheimer's disease in individuals with subjective cognitive decline	Plasma	ABtest-MS: A novel antibody-free mass spectrometry (MS)-based method. Uses liquid chromatography-differential mobility spectrometry-triple quadrupole mass spectrometry (HPLC-DMS-MS/MS)	Plasma Aβ42/40 was 18% lower in PET+ individuals than in PET- individuals	PET	Plasma Aβ42/40 measured by ABtest-MS showed strong potential as a biomarker for early AD detection	-
Allué et al. (2023) [12]	Clinical utility of an antibody-free LC-MS method to detect brain amyloid deposition in cognitively unimpaired individuals from the screening visit of the A4 study	Plasma	Plasma Aβ40 and Aβ42 concentrations were measured using ABtestMS, an antibody-free HPLC-differential mobility spectrometry-triple quadrupole mass-spectrometry (HPLC-DMS-MS/MS) method	Plasma Aβ42/40 was 13.3% lower in PET+ individuals ($p < 0.001$)	Plasma Aβ42/40 alone: AUC = 0.78 (95% CI: 0.75–0.82)	PET	Plasma Aβ42/40 declines before PET detects amyloid plaques, suggesting it may serve as an earlier biomarker
Weber et al. (2024) [16]	Clinical utility of plasma Aβ42/40 ratio by LC-MS/MS in Alzheimer's disease assessment	Plasma	Immunoprecipitation (IP)-LC-MS/MS. Aβ42 and Aβ40 were immunoprecipitated and enzymatically digested using Lys-C	Plasma Aβ42/40 was 18% lower in PET+ individuals than in PET- individuals	Plasma Aβ42/40 alone: AUC = 0.84 (95% CI: 0.79–0.89)	PET	Plasma Aβ42/40 measured by IP-LC-MS/MS showed strong potential as a biomarker for early AD detection

Table 1. *Cont.*

Reference	Study Title	Medium	Measurement Method	**Aβ42/40** (vs. PET)	AUC (95% CI)	Reference Standard	Notes
Meyer et al. (2024) [17]	Clinical validation of the PrecivityAD2 blood test: A mass spectrometry-based test with algorithm combining %p-tau217 and Aβ42/40 ratio to identify presence of brain amyloid	Plasma	Plasma Aβ42 and Aβ40 were quantified using an immunoprecipitation-based LC-MS/MS assay	Aβ42/40 was 12% lower in PET+ individuals	Plasma Aβ42/40 alone: AUC = 0.75 (95% CI: 0.71–0.79, $p < 0.001$))	PET	The combination of % p-tau217 and Aβ42/40 in PrecivityAD2 significantly improves diagnostic accuracy
Zicha et al. (2022) [18]	Comparative analytical performance of multiple plasma Aβ42 and Aβ40 assays and their ability to predict positron emission tomography amyloid positivity	Plasma	Six different Aβ42/40 assays were tested: Three ligand-binding (immunoassays) Three mass spectrometry-based (MS) assays	Lower plasma Aβ42/40 in PET+ individuals compared to PET- individuals	Washington University IP-LC-MS/MS: AUC = 0.814 (95% CI: 0.736–0.892) Roche Elecsys Cobas e601: AUC = 0.710 (95% CI: 0.617–0.803) Shimadzu IP-MALDI-TOF-MS: AUC = 0.715 (95% CI: 0.625–0.805)	PET	Aβ42/40 outperformed Aβ42 or Aβ40 alone for detecting PET amyloid positivity
Schindler et al. (2019) [19]	High-precision plasma β-amyloid 42/40 predicts current and future brain amyloidosis	Plasma and CSF	Plasma Aβ40 and Aβ42: Immunoprecipitation and liquid chromatography–mass spectrometry (IP-LC-MS/MS). CSF Aβ42, t-tau, and p-tau181 were measured using Roche Elecsys immunoassays	Plasma Aβ42/40 was 11% lower in PET+ individuals	Plasma Aβ42/40 alone: AUC = 0.88 (95% CI: 0.82–0.93). CSF Aβ42/40 alone: AUC = 0.98 (95% CI: 0.95–0.99) (Both compare with PET)	PET	Plasma Aβ42/40 measured by IP-LC-MS/MS demonstrated high accuracy for predicting amyloid PET status
Fandos et al. (2017) [1]	Plasma amyloid β42/40 ratios as biomarkers for amyloid β cerebral deposition in cognitively normal individuals	Plasma	Ratio measurement by enzyme-linked immunosorbent assays (ELISAs). Aβ40 and Aβ42 peptides were quantified using Aβ test40 and Aβ test42, respectively (Araclon Biotech Ltd. Zaragoza, Spain)	Lower plasma Aβ42/40 in PET+ individuals compared to PET- individuals	Total Aβ42/40 (TP42/40) model: AUC = 0.79	PET	Plasma Aβ42/40 strongly correlates with amyloid PET SUVR and is a promising pre-screening biomarker for clinical trials. Plasma Aβ42/40 changes before amyloid PET detects amyloid positivity, supporting its role as an early biomarker for AD Different fractions of Aβ (total, bound, free) all showed predictive ability, but total Aβ42/40 (TP42/40) had the strongest performance
Wisch et al. (2023) [20]	Predicting continuous amyloid PET values with CSF and plasma Aβ42/40	Plasma and CSF	CSF Aβ42/40 measured using automated chemiluminescent enzyme immunoassays (Fujirebio LUMIPULSE G1200) Plasma Aβ42/40 measured using an immunoprecipitation-mass spectrometry assay (C2N Diagnostics)	Plasma Aβ42/40 correlated with PET amyloid load (Spearman $\rho = -0.56$), but CSF Aβ42/40 had a stronger correlation ($\rho = -0.73$)	-	PET	CSF Aβ42/40 was a better predictor of continuous amyloid burden than plasma Aβ42/40. ML models improved amyloid PET prediction, with CSF-based models outperforming plasma-based models
Li et al. (2022) [21]	Validation of plasma amyloid-β 42/40 for detecting Alzheimer disease amyloid plaques	Plasma	Measurement Methods: Immunoprecipitation-mass spectrometry (IP-MS) assay developed by C2N Diagnostics	-	Plasma Aβ42/40 alone: AUC = 0.84 (95% CI: 0.80–0.87)	PET	Plasma Aβ42/40 reliably detects amyloid positivity, but CSF Aβ42/40 remains a stronger predictor Plasma Aβ42/40 is more useful as a dichotomous marker (PET+ vs. PET-) than a continuous predictor of amyloid burden

Table 2. Summary of fluorescence-based biomarker studies for Aβ detection.

Reference	Study Title	Biomarker	Aβ	Buffer	λ_{exc}	λ_{em}	Affinity Constant	Fluorescence Change	[Aβ]	Notes
Telpoukhovskaia et al. (2015) [32]	3-Hydroxy-4-pyridinone derivatives designed for fluorescence studies to determine interaction with amyloid protein as well as cell permeability.	HL_{22}	Aβ40	10 mM sodium buffer with 1 mM EDTA at pH 7.4.	310 nm	420 nm	-	50% fluorescence increase in presence of amyloid	230 μM	The % fluorescence increase is after 3 h incubation fibrils
Li et al. (2022) [33]	A multichannel fluorescent tongue for amyloid-β aggregates detection.	Cationic PPE; Thioflavin T (ThT); Nile Red (NR) and Vitoria Blue B (VBB) + Graphene oxide	Aβ40 and Aβ42	PBS and Serum	400, 415, 550, 620 nm	445, 490, 635, 700 nm	-	-	1 μM	100% detection accuracy (PBS) and 91.7% in Serum
Li et al. (2019) [24]	A simple approach to quantitative determination of soluble amyloid-β peptides using a ratiometric fluorescence probe.	Ratiometric fluorescence probe, BPNS-Zn^{2+} complex	Aβ40	20 mM Tris-HCl, 150 mM NaCl, 5% v/v MeOH, pH 7.4	332 nm	505 nm (decrease), 423 nm (increase)	BPNS-Zn^{2+}: 4.11×10^6 M^{-1} in 10 mM Tris buffer	Upon addition of Aβ40, the quenched fluorescence at 505 nm was recovered, and the peak at 423 nm diminished. The quantum yield increased from 0.060 (BPNS-Zn^{2+}) to 0.160 upon binding to Aβ40. The ratiometric fluorescence ratio (F_{505}/F_{423}) increased in a concentration-dependent manner for Aβ40 monomers. Aβ40 monomers induced a much stronger fluorescence change than protofibrils and fibrils, confirming the stronger affinity of Zn^{2+} for soluble Aβ species.	Aβ40 monomer concentration range was 0–7 μM for fluorescence titration experiments, with a detection limit of 390 nM. The fluorescence assay was calibrated in the range of 0–100 μM	Ratiometric IF_{505}/IF_{423} measurement. Possible interference of other proteins was checked.

Table 2. *Cont.*

Reference	Study Title	Biomarker	Aβ	Buffer	λ_{exc}	λ_{em}	Affinity Constant	Fluorescence Change	[Aβ]	Notes
Lv et al. (2016) [34]	A spiropyran-based fluorescent probe for the specific detection of β-amyloid peptide oligomers in Alzheimer's disease.	AN-SP	Aβ42	PBS (pH 7.31)	430 nm	557 nm (ANCA unit fluorescence); 701 nm (slightly open form of AN-SP in PBS)	1.7 μM - K_d AN-SP for Aβ oligomers	Upon binding to Aβ oligomers, the fluorescence at 540 nm increased by a factor of 9.4. The quantum yield increased significantly: From 0.98% (free AN-SP) to 16.3% (Aβ oligomer-bound).	Aβ oligomers were used at 5 μM. The linear detection range for Aβ oligomers was 0–12 μM, with a high correlation (R^2 = 0.988)	AN-SP demonstrated high selectivity for Aβ oligomers over other amyloidogenic proteins, including: Amylin Prion protein fragments (PrP 106–126). AN-SP penetrates the blood-brain barrier (BBB) and specifically labels Aβ oligomers in the brains of AD transgenic mice. AN-SP fluorescence colocalized with Aβ oligomer-specific antibodies, confirming its specificity in both in vitro and in vivo studies. AN-SP was non-toxic (cell viability remained >90% at 1–100 μM concentrations in MTT assays).
Nabers et al. (2016) [35]	Amyloid-β-secondary structure distribution in cerebrospinal fluid and blood measured by an immuno-Infrared-Sensor: A biomarker candidate for Alzheimer's disease	The method monitored the secondary structure distribution of Aβ in CSF and blood plasma. The immuno-infrared sensor detects β-sheet-rich Aβ conformations, which are associated with misfolded and aggregated forms of Aβ in AD patients.	Aβ40 and Aβ42	CSF and EDTA blood plasma samples were analyzed directly without additional buffers.	-	-	-	-	-	The amide I band (1700–1600 cm^{-1}) was analyzed to assess the secondary structure of Aβ peptides. the amide I band shift was used as a diagnostic marker: CSF samples from DAT patients showed an amide I band shift to lower wavenumbers (∼1640 cm^{-1}), indicating increased β-sheet content. Blood plasma samples exhibited a similar but less pronounced shift (∼1642 cm^{-1}).

Table 2. *Cont.*

Reference	Study Title	Biomarker	Aβ	Buffer	λ_{exc}	λ_{em}	Affinity Constant	Fluorescence Change	[Aβ]	Notes
Mora et al. (2016) [36]	Benzothiazole-Based Neutral Ratiometric Fluorescence Sensor for Amyloid Fibrils	2Me-DABT	Insulin amyloid fibrils were prepared by incubating 2 mg/mL insulin in 25 mM HCl, 100 mM NaCl (pH 1.6) at 65 °C for 4 h	Amyloid fibrils were initially prepared in an acidic medium (pH 1.6, 25 mM HCl, 100 mM NaCl). Fibrillar solutions were then diluted 12-fold with Tris-HCl buffer and adjusted to pH 7.4 using NaOH before fluorescence measurements	340 nm	500 nm (free 2Me-DABT in aqueous solution) 445 nm (2Me-DABT bound to amyloid fibrils)	Two distinct binding modes were observed, leading to two different binding constants: Strong binding mode: 1.0×10^6 M^{-1}; Weaker binding mode: 4.1×10^4 M^{-1};	Emission intensity increased ~65× upon binding to amyloid fibrils. Large hypsochromic (blue) shift from 500 nm to 445 nm occurred upon amyloid binding. Quantum yield increased from 0.02 (free) to 0.68 (bound to fibrils). Time-resolved fluorescence measurements showed an increase in the average fluorescence lifetime from 2.9 ns (free) to 4.3 ns (bound). Unlike ThT, 2Me-DABT fluorescence shift allows ratiometric detection, reducing background noise in imaging applications	Insulin amyloid fibrils were used at concentrations of 0–30 μM for fluorescence titration experiments	-
Ran et al. (2020) [37]	CRANAD-28: A robust fluorescent compound for visualization of amyloid beta plaques	CRANAD-28	Aβ peptides targeted: Aβ monomers Aβ dimers Aβ oligomers Aβ plaques (in ex vivo and in vivo imaging)	PBS (pH 7.4)	498 nm	578 nm	-	CRANAD-28 fluorescence intensity increased significantly upon binding Aβ plaques, resulting in higher signal-to-noise ratio (SNR = 5.54) compared to Thioflavin S (SNR = 4.27)	-	CRANAD-28 has the excitation/emision peak on 498/578 nm in PBS solution
Zhou et al. (2019) [38]	Environment-sensitive near-infrared probe for fluorescent discrimination of Aβ and tau fibrils in AD brain	3 different dyes "16; 17 and 18"	Aβ42	PBS (phosphate-buffered saline, pH 7.4) with 10% ethanol (EtOH) was used for spectral measurements	16: 568 nm without Amyloid - 560 nm with Amyloid; 17: 570 nm without Amyloid - 564 nm with Amyloid; 18: 572 nm without Amyloid - 582 nm with Amyloid	16: 646 nm without Amyloid - 583 nm with Amyloid; 17: 695 nm without Amyloid - 618 nm with Amyloid; 18: 762 nm without Amyloid - 650 nm with Amyloid	16: 182.2 nM; 17: 131.1 nM; 18: 43.1 nM	Fluorescence enhancement fold upon interaction with the Aβ42: 16: 21.7; 17: 33.5; 18: 222.6	1.95 μM	-

Table 2. *Cont.*

Reference	Study Title	Biomarker	Aβ	Buffer	λ_{exc}	λ_{em}	Affinity Constant	Fluorescence Change	[Aβ]	Notes
Chen et al. (2022) [39]	Fluorescent aptasensor based on conformational switch–induced hybridization for facile detection of β-amyloid oligomers	Fluorophore-labeled aptamer (FAM-Apt) specifically binds Aβ oligomers (AβO)		Phospate buffer (pH 7.4)	488 nm	520 nm	The aptamer (Apt) used in the study has a K_d = 25 nM for AβO (previously reported by Tsukakoshi et al.)	Fluorescence decreases upon AβO binding The aptamer undergoes a conformational switch (G-quadruplex → Apt-AβO binding complex) This increases hybridization efficiency with complementary DNA-magnetic beads (cDNA-MBs), which reduces fluorescence intensity Fluorescence intensity vs. AβO concentration follows a linear inverse relationship	Final concentration range: 1.7 ng/mL–85.1 ng/mL Limit of detection (LOD): 0.87 ng/mL Linear detection range: 1.7 ng/mL–85.1 ng/mL (R^2 = 0.9977)	Highly selective for AβO: Negligible response to monomeric or fibrillar Aβ Minimal interference from plasma proteins (HSA, BSA)
Du et al. (2024) [25]	Machine learning-assisted fluorescence/fluorescence colorimetric sensor array for discriminating amyloid fibrils	Thioflavin T (ThT); Congo Red (CR); 8-anilino-1-naphthalenesulfonic acid (ANS); Safranine T (ST), berberine (BBR) and coptisine (Cs)	Aβ42	NaOH-PBS buffer for Aβ42 fibrils	Tht: 432 nm without Amyloid/436 nm with Amyloid; CR: 507 nm without Amyloid - 500 nm with Amyloid; ANS: 359 nm without Amyloid - 370 nm with Amyloid; ST: 554 nm without Amyloid - 555 nm with Amyloid; BBR: 348 nm without Amyloid - 356 nm with Amyloid; Cs: 357 nm without Amyloid - 357 nm with Amyloid	Tht: 488 nm without Amyloid/484 nm with Amyloid; CR: 612 nm without Amyloid - 600 nm with Amyloid; ANS: 526 nm without Amyloid - 493 nm with Amyloid; ST: 577 nm without Amyloid - 577 nm with Amyloid; BBR: 530 nm without Amyloid - 522 nm with Amyloid; Cs: 548 nm without Amyloid - 546 nm with Amyloid	-	Fluorescence response factor (F/F0): ThT: 7.38; CR: 3.15; ANS: 1.79; ST: 2.63; BBR: 2.84; Cs: 1.07	The quantification range for individual amyloid fibrils was: Fluorescence sensor array: 0.05–5 μM; Fluorescence colorimetric array: 0.5–10 μM	LOD for Aβ42 fibrils (Aβ-F): 14.57 nM

Table 2. *Cont.*

Reference	Study Title	Biomarker	Aβ	Buffer	λ_{exc}	λ_{em}	Affinity Constant	Fluorescence Change	[Aβ]	Notes
Freire et al. (2014) [40]	Photophysical study of Thioflavin T as fluorescence marker of amyloid fibrils	Thioflavin T	Aβ42	Phosphate-buffered saline (PBS), pH 7.2, with 150 mM NaCl was used for preparing amyloid samples	350; 375 and 410 nm	402 nm (excitation at 350 nm); 472–482 nm (excitation at 375–410 nm)	5.85×10^3 M^{-1}	Fluorescence quantum yield: 0.00033 in buffer (free form) 0.31 when bound to Aβ fibrils	Aβ1–42 fibril concentration: 138 μM. ThT concentrations tested: 1.1 μM and 7.0 μM (fluorescence experiments) 244 μM (absorption measurements)	-
Xue et al. (2017) [41]	Thioflavin T as an Amyloid Dye: Fibril Quantification, Optimal Concentration, and Effect on Aggregation	Thioflavin T	Aβ40 and Aβ42	PBS	450 nm	490 nm	-	-	Aβ40: 40 μM Aβ42: 15 μM	Maximum fluorescence observed at ThT concentrations of 20–50 μM. At concentrations $\geq$ 5 μM, ThT exhibits self-fluorescence due to micelle formation
Dos Santos et al. (2022) [26]	Alzheimer's disease diagnosis by blood plasma molecular fluorescence spectroscopy (EEM)	NADH (Nicotinamide Adenine Dinucleotide); Tyrosine residues in Aβ1–40 aggregates Glycated Aβ amyloid (AGE-Aβ)	Aβ40	-	250, 260, 340 nm	399, 470 nm	-	-	-	A noticeable decrease in fluorescence intensity was observed between 360 and 470 nm in AD patients. Possible reasons for fluorescence change: Mitochondrial dysfunction affecting NADH fluorescence; Tyrosine fluorescence shifts associated with Aβ1–40 aggregates; Decreased fluorescence due to protein glycation and oxidative stress. Key Observations: NADH fluorescence (250–260 nm excitation, 470 nm emission) was altered in AD plasma. Tyrosine fluorescence (340 nm excitation, 399 nm emission) linked to Aβ1–40 and AGE-Aβ. The fluorescence intensity differences between AD and controls were significant enough for 94.12% classification accuracy using ML models.

Table 3. Summary of application of AI and ML in Aβ detection.

Reference	Study Title	AI/ML Method Used	% Training Set and % of Test Set	Data Type	Performance Metrics	Key Findings
Han et al. (2024) [27]	A machine learning algorithm based on circulating metabolic biomarkers offers improved predictions of neurological diseases	eXtreme Gradient Boosting (XGBoost) Random Forest Logistic Regression 10-fold Cross-Validation was used for model training and validation	70% and 30%	Circulating metabolic biomarkers (NMR spectroscopy-detected). Clinical risk factors (age, sex, education, BMI, alcohol consumption, work status, frequency of social visits, blood pressure, history of hypertension, diabetes); Neurological disease data (Dementia, Parkinson's disease (PD), and AD) UK Biobank dataset with 62,393 participants	AUC: Dementia: 0.841 (Metabolic model), 0.823 (Clinical model), 0.940 (Combined model) AD: 0.928 (Metabolic model), 0.880 (Clinical model), 0.948 (Combined model) PD: 0.902 (Metabolic model), 0.826 (Clinical model), 0.913 (Combined model) Net Reclassification Improvement (NRI): Dementia: 0.159 AD: 0.113 PD: 0.201 Integrated Discrimination Improvement (IDI): Dementia: 0.098 AD: 0.070 PD: 0.085	XGBoost outperformed Random Forest and Logistic Regression for predicting neurological diseases. Metabolic biomarkers significantly improved the predictive power over clinical models alone. Combining metabolic biomarkers with clinical data provided the highest predictive accuracy for all three neurological diseases
Karaglani et al. (2020) [28]	Accurate blood-based diagnostic biosignatures for Alzheimer's disease via automated machine learning	Automated Machine Learning (AutoML) via Just Add Data Bio (JADBIO); Support Vector Machines (SVM); Random Forest; Ridge Logistic Regression; Bootstrap Bias Corrected Cross-Validation (BBC-CV) for performance estimation	70% and 30%	Blood-based multi-omics data (miRNA, mRNA, and proteomic datasets) Publicly available datasets (BioDataome, Metabolomics Workbench, GEO repositories) Patients: AD and age/sex-matched cognitively healthy individuals	miRNA-Based Model (SVM) AUC: 0.975 (95% CI: 0.906–1.000) Features: 3 miRNA predictors mRNA-Based Model (Random Forest) AUC: 0.846 (95% CI: 0.778–0.905) Features: 25 mRNA predictors Protein-Based Model (Ridge Logistic Regression) AUC: 0.921 (95% CI: 0.849–0.972) Features: 7 protein predictors	AutoML identified the most predictive biosignatures from miRNA, mRNA, and proteomic data. The miRNA-based model had the highest accuracy (AUC: 0.975) and required only 3 feature. Findings suggest that blood-based biomarkers can be used for minimally invasive AD diagnosis. AutoML helped reduce dimensionality while preserving accuracy, making the biomarkers more clinically feasible
Xu et al. (2022) [29]	Alzheimer's disease diagnostics using miRNA biomarkers and machine learning	Multilayer Perceptron (MLP) Random Forest (RF) Random Tree (RT) Naïve Bayes (NB) Bootstrap Bias Corrected Cross-Validation (BBC-CV) for performance estimation	70% and 30%	miRNA biomarkers from blood samples (serum and plasma) Dataset based on dysregulated miRNA associated with AD miRNA expression profiles from published datasets Genomic attributes (target genes) and pathway attributes (biological pathways) used as ML feature	Serum-Based Model (MLP Classifier) Accuracy: 92.0% Features: 704 filtered miRNA descriptors Plasma-Based Model (RF Classifier) Accuracy: 90.9% Features: 54 filtered miRNA descriptors. Additional Validation with Independent Testing Sets: Serum Model (with MLP): "Clean" test set accuracy: 83.3% "Natural" test set accuracy: 88.9% Plasma Model (with RF): "Clean" test set accuracy: 78.6% "Natural" test set accuracy: 85.7%	ML models using miRNA biomarkers successfully differentiated AD from healthy individuals with high accuracy. Serum and plasma miRNA datasets performed similarly but required separate models due to different molecular compositions. miRNA profiling allowed for a non-invasive approach to AD diagnosis, outperforming many traditional methods. Feature selection using genomic targets and pathway attributes improved classification accuracy

Table 3. *Cont.*

Reference	Study Title	AI/ML Method Used	% Training Set and % of Test Set	Data Type	Performance Metrics	Key Findings
Dos Santos et al. (2022) [26]	Alzheimer's disease diagnosis by blood plasma molecular fluorescence spectroscopy (EEM)	Parallel Factor Analysis with Quadratic Discriminant Analysis (PARAFAC-QDA) Tucker3 with Quadratic Discriminant Analysis (Tucker3-QDA) Multivariate Analysis of Excitation-Emission Matrix (EEM) fluorescence spectroscopy	PARAFAC-QDA: Training: 91.52%	Fluorescence spectroscopy data from blood plasma samples 230 individuals (83 AD patients, 147 healthy controls) Excitation-Emission Matrix (EEM) Fluorescence Spectroscopy	PARAFAC-QDA Model: Accuracy: 94.12% Sensitivity: 83.33% Specificity: 100% Precision: 100% F2-score: 86.21% Matthews Correlation Coefficient (MCC): 0.87 Test Effectiveness (δ): ∞ (very high discrimination power) Tucker3-QDA Model: Accuracy: 94.12% Sensitivity: 91.67% Specificity: 95.45% Precision: 91.67% F2-score: 91.67% MCC: 0.87 Test Effectiveness (δ): 3.00 (high discrimination power)	Fluorescence spectroscopy combined with ML successfully differentiated AD patients from healthy controls. EEM fluorescence detected spectral changes in NADH, tyrosine residues in amyloid-beta (Aβ), and mitochondrial dysfunction. Tucker3-QDA slightly outperformed PARAFAC-QDA in sensitivity, making it more effective at detecting AD cases. PARAFAC-QDA exhibited higher specificity and discrimination power, minimizing false positives. Feature selection using fluorescence excitation and emission wavelengths improved model interpretability. This method provides a rapid, cost-effective, and minimally invasive alternative to traditional AD diagnostics
Du et al. (2024) [25]	Machine learning-assisted fluorescence/fluorescence colorimetric sensor array for discriminating amyloid fibrils	Linear Discriminant Analysis (LDA) Principal Component Analysis (PCA) Hierarchical Cluster Analysis (HCA) ML-assisted Fluorescence/Fluorescence Colorimetric Sensor Array	-	Fluorescence and fluorescence colorimetric sensor array. Amyloid fibril detection from biological fluids	Fluorescence Sensor Array (Array B - LDA) Accuracy: 100% (amyloid fibrils correctly identified). Fluorescence Colorimetric Sensor Array (Array D - LDA) Accuracy: 96–100% (high selectivity for amyloid fibrils)	ML-enhanced fluorescence sensor array successfully identified amyloid fibrils with high sensitivity. Fluorescence intensity (Array B) and fluorescence colorimetric changes (Array D) provided complementary detection methods. Array B exhibited superior sensitivity and selectivity, detecting amyloid fibrils at sub-nanomolar concentrations. Array D enabled rapid, smartphone-based visual detection for practical, low-cost diagnostics. Dimensionality reduction using PCA optimized the sensor arrays while maintaining high discrimination accuracy. Validated in biological matrices (diluted human plasma and aCSF), showing real-world applicability. Potential for early Alzheimer's disease diagnosis through Aβ detection. Capability to differentiate binary amyloid fibril mixtures, relevant for mixed proteinopathie

Table 3. *Cont.*

Reference	Study Title	AI/ML Method Used	% Training Set and % of Test Set	Data Type	Performance Metrics	Key Findings
Li et al. (2022) [33]	A multichannel fluorescent tongue for amyloid-β aggregates detection	Linear Discriminant Analysis (LDA) Principal Component Analysis (PCA) for feature selection K-Nearest Neighbors (KNN) Random Forest (RF) Logistic Regression (LR) Generalized Predictive Control (GPC) Branch and Bound (BnB) 10-fold Cross-Validation for performance estimation	60% and 40%	Multichannel Fluorescence Sensor Array Detection of Aβ aggregates in PBS and serum	Different ML Methods: Best in PBS samples: LDA & RF (accuracy 97.2%) Best in Serum samples: KNN (accuracy 95.8%)	Multichannel fluorescence sensor array successfully discriminated Aβ42/Aβ40 aggregates. Feature reduction with PCA led to a 6-channel optimized array, maintaining high accuracy. ML optimized the detection system, with RF and KNN yielding the best accuracy

Table 4. Cohorts comparation of studies on Aβ42/40 summarized in Table 1.

Reference	Cohort
West et al. (2021) [22]	414 plasma sample, where: 253 was PET- (79.8% CDR = 0) 161 PET+ (32% CDR = 0)
Gao et al. (2022) [15]	326 participants: 96 CN 94 MCI 107 EOAD 66 LOAD 48 non Alzheimer's dementia
Udeh-Momoh et al. (2022) [14]	115 participants. AUC and cut-off calculated for CU individuals
Pascual-Lucas et al. (2023) [13]	200 healthy individuals with SCD, of wich 36 (18%) were PET+
Allué et al. (2023) [12]	CU individuals
Weber et al. (2024) [16]	250 participants: 72 HC (5 PET+ and 67 PET-) 124 MCI (42 PET+ and 82 PET-) 54 AD (all PET+)
Meyer et al. (2024) [17]	583 samples: 476 MCI (81.6%) 107 Dementia (18.4%)
Zicha et al. (2022) [18]	121 individuals (60 PET+ and 61 PET-) 49 CN (18 PET+ and 31 PET-) 54 MCI (26 PET+ and 28 PET-) 18 AD (16 PET+ and 2 PET-)
Schindler et al. (2019) [19]	158 participants mostly CN (43 PET+ and 115 PET-): 94% CDR = 0
Fandos et al. (2017) [1]	All CN
Wisch et al. (2023) [20]	491 individuals (157 PET+ and 334 PET-): 87% CDR = 0
Li et al. (2022) [21]	465 participants 170 CN 46 SMC or SCD 203 MCI 46 AD

Abbreviations: CN = Cognitively Normal; MCI = Mild Cognitive Impairment; EOAD = Early-Onset AD; LOAD = Late-Onset AD; AD = Alzheimer's Disease; PET = Positron Emission Tomography; HC = Healthy Controls; CU = Cognitively Unimpaired; CDR = Clinical Dementia Rating; SCD = Subjective Cognitive Decline; SMC= Significant Memory Concern AUC = Area Under the Curve.

4. Discussion

4.1. Analysis of Plasma and CSF Aβ42/40 Across Studies and Its Relationship to PET Diagnosis

The studies reviewed collectively highlight the potential of plasma Aβ42/40 as a non-invasive biomarker for identifying amyloid pathology in AD, though with varying degrees of sensitivity, specificity, and correlation with standard amyloid PET and CSF biomarkers.

Across all studies, plasma Aβ42/40 consistently showed a significant reduction in amyloid PET+ individuals compared to PET- individuals, with differences typically ranging from 7% to 18% lower in PET+ participants. However, the degree of separation varied depending on the analytical platform used. Studies that employed high-precision mass spectrometry (MS)-based assays consistently achieved higher diagnostic accuracy compared to studies using immunoassay-based techniques (mean AUC of 0.80 and 0.71 respectively), see Table 1. The most significant reduction observed in Aβ42/40 of PET+ individuals with respect to PET- ones was 18% in the work of Pascual et al. [13] and Weber et al. [16] using a novel antibody-free mass spectrometry (MS) and an immunoprecipitation (IP)-LC-MS/MS respectively.

Genetic factors influencing biomarker performance. Importantly, genetic predisposition significantly modulates plasma biomarker accuracy. Some studies analyzed the

presence of Apolipoprotein (APoE). The APOE gene plays a role in lipid transport and is closely linked to AD risk. It has several alleles, with APOE ϵ2 potentially offering some protection and delaying onset, found in approximately 5–10% of individuals. APOE ϵ3, the most common form, is considered neutral, neither increasing nor decreasing risk. In contrast, APOE ϵ4 is associated with a higher risk and earlier onset of Alzheimer's, present in 15–25% of people, with 2–5% carrying two copies [42].The presence of APOE improved the AUC value in all studies in which it was used (see Table 1), reinforcing the role of genetic predisposition in modifying plasma biomarker performance. Some of these studies also used the age and/or sex for diagnostic.

It is important to note that a small subset of AD cases (<1%) follows an autosomal-dominant inheritance pattern and has an earlier age at onset than sporadic AD. These familial forms are driven by pathogenic mutations in the presenilin 1/2 (PSEN1/PSEN2) or amyloid precursor protein (APP) genes, which shift γ-secretase cleavage toward the more aggregation-prone Aβ42 species [43,44]. Among the studies we reviewed, only Zhou et al. (2019) [38] stratified their experiments using APP/PSEN1 transgenic mice to validate probe 18, directly demonstrating how these mutations affect assay sensitivity. The remaining studies, while critical for evaluating amyloid detection technologies, assess biomarkers in AD cohorts without distinguishing etiology.

Analytical variability and calibration challenges. Cut-off values for plasma Aβ42/40 varied dramatically across studies (0.06–0.303, Table 5), reflecting methodological differences that limit direct comparison and clinical standardization.

The observed cut-off variability reflects differences in analytical techniques, including detection of full-length versus truncated Aβ species, sample preparation methods, and calibration approaches [13].

Calibration approaches varied between synthetic solutions [16,17,22] and human plasma matrices [12,13,19], with isotope-labeled internal standards providing the most accurate quantification.

These methodological variations highlight a critical barrier to clinical translation: the absence of standardized protocols prevents the establishment of universal diagnostic thresholds, limiting immediate clinical utility despite promising individual study results.

Together, these factors underscore the need for caution when interpreting and comparing cut-off values from different studies.

Pre-analytical variables can markedly affect Aβ42/40 stability, yet only six studies [12,13,17,19,21,22] report collection and processing details. All used EDTA tubes for plasma—with some directly comparing EDTA versus heparin—and Li et al. additionally examined differences in collection sites and centrifugation speed/time. None specified processing delays, but these omissions did not appear to impact performance: all studies achieved AUCs > 0.75, and the percent differences between amyloid positive and amyloid negative groups remained consistent (see Table 1). Nonetheless, standardizing and reporting these pre-analytical factors is important to improve assay reproducibility and cross-study comparisons.

Recent evidence indicates that a subset of extracellular Aβ—particularly Aβ42—is selectively packaged into exosomes, the small vesicles derived from endosomes involved in intercellular communication [45,46]. None of the studies included in this review have assessed how exosome-associated influences Aβ measured Aβ42/40 in plasma or CSF. We therefore recommend that future biomarker investigations incorporate an EV-fractionation step prior to Aβ quantification to fully capture both free and vesicle-associated species.

Comparative performance with emerging biomarkers. CSF Aβ42/40 consistently outperformed plasma measures, showing larger reductions in PET+ individuals (≈50% vs. 7–18%) and superior diagnostic accuracy [15,19,20,47].

Table 5. Reported mean and cut-off values of Aβ42/40 in plasma.

Reference		Mean Aβ42/40 in Plasma			% Amyloid Positive	Cut-Off Value *
	Comment	One group	CN/CU	AD		
West et al. (2021) [22]		0.097 ± 0.011			39	Plasma Aβ42/40 cutoff value: 0.0975
Gao et al. (2022) [15]			0.07 ± 0.02	0.05 ± 0.02		Cut-off only for CSF Aβ42/40: 0.0642
Udeh-Momoh et al. (2022) [14]	IP-MS: WashU		0.313 ± 0.009	0.199 ± 0.006	91.7 for AD individuals	Cut-off values for PET positivity based on Youden index
	IP-MALDI-TOF-MS-Shimadzu		0.043 ± 0.008	0.035 ± 0.005		Shimadzu (MS-based): 0.040 (sensitivity = 73.7%, specificity = 58.6%)
	IP-MS:Gothenburg		0.074 ± 0.019	0.066 ± 0.016		WashU (MS-based): 0.125 (sensitivity = 68.4%, specificity = 82.8%)
	IA: ADx		0.050 ± 0.010	0.046 ± 0.008		
	IA: Quanterix		0.041 ± 0.006	0.036 ± 0.004		Quanterix (IA-based): 0.038 (sensitivity = 68.4%, specificity = 72.4%)
	IA: Roche		0.0171 ± 0.020	0.163 ± 0.029		Roche (IA-based): 0.168 (sensitivity = 84.2%, specificity = 58.6%)
			Aβ PET-	Aβ PET+		
Pascual-Lucas et al. (2023) [13]			0.261 (0.244–0.279)	0.215 (0.203–0.236)		Cut-off for PET positivity based on Youden index: Aβ42/40 = 0.241
Allué et al. (2023) [12]			0.30 (0.27–0.33)	0.26 (0.23–0.28)		Optimal cut-off for PET positivity based on Youden index: Aβ42/40 = 0.303
Weber et al. (2024) [16]			0.173 ± 0.029	0.141 ± 0.017		Optimal cut-off for PET positivity based on Youden index: Aβ42/40 = 0.160
Meyer et al. (2024) [17]			0.1001 ± 0.0150	0.0878 ± 0.0101		Aβ42/40 cut-off: Optimal cut-off = 0.094 (slightly higher than previous studies: 0.089
Zicha et al. (2022) [18]	Washington University		0.133 ± 0.010	0.123 ± 0.008		Aβ42/40 cut-offs varied by assay: Washington University (MS): 0.133 (PET-) vs. 0.123 (PET+)
	Scimadzu		0.042 ± 0.007	0.037 ± 0.005		Shimadzu (MS): 0.042 (PET-) vs. 0.037 (PET+)
	Roche		0.168 ± 0.022	0.153 ± 0.022		Roche (IA): 0.168 (PET-) vs. 0.153 (PET+)
	University of Gothenburg		0.072 ± 0.017	0.064 ± 0.023		University of Gothenburg (MS): 0.072 (PET-) vs. 0.064 (PET+)
	ADx NeuroSciences		0.049 ± 0.010	0.044 ± 0.007		ADx NeuroSciences (IA): 0.049 (PET-) vs. 0.044 (PET+)
	Quanterix		0.040 ± 0.006	0.038 ± 0.004		Quanterix (IA): 0.040 (PET-) vs. 0.038 (PET+)
Schindler et al. (2019) [19]			0.128 ± 0.009	0.115 ± 0.006		Optimal cut-off for PET positivity: Plasma Aβ42/40 < 0.1218 Alternative reference cut-off for CSF Aβ42/40: CSF Aβ42/40 < 0.1094
Fandos et al. (2017) [1]	m18		0.083 ± 0.028	0.068 ± 0.020		Plasma Aβ42/40 cut-off for PET positivity: TP42/40 (Total Plasma Aβ42/40) < 0.068 BP42/40 (Bound Plasma Aβ42/40) < 0.067 FP42/40 (Free Plasma Aβ42/40) < 0.066. For m18, 18 month visit
	m36		0.088 ± 0.024	0.071 ± 0.027		
	m54		0.085 ± 0.034	0.067 ± 0.015		
Wisch et al. (2023) [20]			0.104 ± 0.008	0.094 ± 0.007		Plasma Aβ42/40 cut-off for PET positivity: Optimal cut-off = 0.094 CSF Aβ42/40 cut-off for PET positivity: Optimal cut-off = 0.046
Li et al. (2022) [21]			0.131 ± 0.011	0.118 ± 0.009		Plasma: 0.123 for AIBL and BioFINDER to 0.125 for ADNI

* The cut-off values are indicated for plasma, otherwise, if they are measured for CSF, it is indicated in each work.

One work also mentions the high concordance of Aβ42/40 in CSF with tTau and pTau measurements, rather than just using Aβ42 concentration [48]. Wisch et al. [20] demonstrates that CSF Aβ42/40 correlates more strongly with amyloid PET centiloid values ($\rho = -0.73$) than plasma Aβ42/40 ($\rho = -0.56$), suggesting that plasma biomarkers capture amyloid pathology less precisely.

Temporal dynamics and early detection potential. Some analyses [1,7,12,13,19,21,22,49,50] suggest that plasma Aβ42/40 may become abnormal before amyloid PET detects amyloid aggregates (see Table 1). Several studies further support this, showing that plasma Aβ42/40 declines before amyloid PET positivity, a pattern also observed with p-tau231, reinforcing the role of plasma Aβ42/40 in detecting early amyloid pathology. Janelidze et al. [49] found that plasma Aβ42/40 has comparable diagnostic accuracy to p-tau231 in cognitively unimpaired (CU) individuals (AUC 0.79 for Aβ42/40 and AUC 0.71–0.83 for p-tau231), underscoring its potential in early detection. However, both Aβ42/40 and p-tau231 exhibit early cross-sectional changes in response to amyloid pathology, but eventually reach a plateau, limiting their utility in monitoring disease progression over time. This suggests that plasma Aβ42/40 and p-tau231 function primarily as state markers, effectively distinguishing between amyloid-positive and amyloid-negative individuals, but lacking the capacity to determine the stage or rate of disease progression [7,49,50].

Several other minimally invasive biomarkers also show promise, such as Glial Fibrillary Acidic Protein (GFAP), Neurofilament Light Chain (NfL), and Phosphorylated-tau-181 (pTau 181); these biomarkers provide complementary information on astrocytic activation, tau pathology, and neuroaxonal injury as the disease progresses [51,52].

4.2. Fluorescence-Based Amyloid Detection Methods

The studies reviewed employ a variety of fluorescence-based strategies to detect and characterize amyloid fibrils, oligomers, and other aggregated protein species relevant to neurodegenerative diseases such as AD. Approaches include classical dyes (e.g., Thioflavin T, ThT), ratiometric and near-infrared (NIR) probes, sensor arrays, and ML-assisted detection systems. Table 2 compares methodologies, excitation/emission wavelengths, binding affinities, changes in quantum yield, and other key performance metrics.

Classical markers such as ThT (see [40,41]) show a marked fluorescence enhancement on binding to β-sheet-rich fibrils and thus remain useful indicators of fibrillar amyloid. However, ThT is insensitive to oligomeric species, can self-aggregate at high concentrations, and is subject to experimental variability [40,41]; these limitations have driven the development of probes with greater selectivity for oligomers and improved photophysical properties.

Evolution from traditional markers to advanced probe design. As noted above, several fluorescent probes are discussed in the studies reviewed here. Telpoukhovskaia et al. [32] investigated the compound HL_{22} and reported a 50% increase in fluorescence intensity on binding to amyloid fibrils, with an emission maximum at 420 nm. Mora et al. [36] examined 2Me-DABT and demonstrated ratiometric fluorescence detection with a pronounced blue shift (500–445 nm) on fibril binding, making this probe more reliable than ThT for quantitative applications. A 2019 study described an NIR probe that exhibited a marked shift in emission from 762 nm to 650 nm upon addition of Aβ; this probe may be particularly useful for distinguishing Aβ plaques from tau neurofibrillary tangles (NFTs), an important diagnostic distinction in AD [38].

Other probes have been applied to labeled brain sections and compared with ThT. CRANAD-28 was used to stain mounted brain sections to assess plaque-labeling quality and robustness [37]; an antibody (3D6) served as the control. Compared with ThT, CRANAD-28 labeled more plaques: the mean diameter of the labeled zone was 14, 18, and 20 µm for

ThT, CRANAD-28 and 3D6, respectively. One plausible explanation for the larger labelled area with CRANAD-28 is that it can bind smaller Aβ species, including soluble monomers and oligomers, thereby producing a wider staining halo.

Novel fluorescent probes with enhanced specificity. All probes mentioned before, (HL_{22}, 2Me-DABT, Probe 18 of Zhou, and CRANAD-28) offer significant improvements compared to ThT in binding specificity, fluorescence response, and clinical applicability, with several showing blood-brain barrier (BBB) penetration, making them potential candidates for in vivo imaging of amyloid plaques. Moreover, ThT cannot be employed for in vivo imaging due to its positive charge, which makes it highly hydrophilic and prevents it from crossing the BBB.

Oligomer-specific detection advances. While many studies focus on mature fibrils, the ability to detect Aβ oligomers is increasingly recognized as a major advancement in amyloid research, given their higher neurotoxicity. Lv et al. [34] introduced AN-SP, a spiropyran-based probe that selectively binds to AβO over fibrils. Unlike ThT and other fibril-preferring dyes, AN-SP exhibited a 9.4-fold fluorescence enhancement upon binding to AβO within a detection range of 0–12 μM, making it a promising candidate for the early detection of AD.

In contrast, Li et al. [24] developed a BPNS-Zn^{2+} fluorescent complex, which shows a quenched fluorescence at 505 nm upon Aβ binding that recovers upon dissociation of oligomers at 423 nm, allowing a ratiometric approach to track AβO formation.

Chen et al. [39] introduced a fluorescent aptasensor, FAM-Apt, capable of detecting AβO in a range of 1.7 to 85.1 ng/mL in plasma. The detection principle involves the presence of FAM-Apt in the reaction buffer, followed by the addition of AβO and cDNA-modified magnetic beads (cDNA-MBs). The aptamer binds specifically to the oligomers, forming an Apt-AβO complex. A magnetic field is then applied to extract the trapped complexes, and the fluorescence intensity of the buffer is measured before and after the procedure to quantify Aβ O.

Furthermore, Li et al. [53] developed F-SLOH, an oligomer-selective cyanine dye. When compared to ThT, F-SLOH demonstrated a significant increase in fluorescence intensity in the presence of AβO (10 μM, 2-hour incubation), with fluorescence decreasing as fibrils formed.

Advanced detection platforms. Some works, like Zhou et al. [38] look for dyes with emission in the near-infrared (NIR) to improve in vivo imaging, or use multiple excitation-emission channels [25,33] to enable more robust fluorescence-based differentiation of amyloid aggregates. Even ratiometric probes were tested with 2Me-DABT and BPNS-Zn^{2+} [24,36] to reduce false positives from background fluorescence.

Other dyes like, Congo Red (CR), 8-anilino-1-naphthalenesulfonic acid (ANS), Safranine T (ST), berberine (BBR), and coptisine in Du et al. [25] were tested for detection of amyloid fibrils and cationic PPE, Nile Red (NR) and Victoria Blue B (VBB) in Li et al. [33] for monomers, oligomers, fibrils.

In this review, no studies have been found that utilize the intrinsic fluorescence of amyloids for the detection of their aggregates. Only the work by dos Santos et al. [26] analyzed the fluorescence of blood plasma samples using chemometric methods as a diagnostic tool for Alzheimer's disease (AD), although they did not specifically address the fluorescence associated with the amyloid proteins themselves or their potential aggregates. Our group has recently published the first observation of Ab40 oligomers through their autofluorescence, particularly marked by the appearance of an aggregation-induced emission (AIE) band in the visible region of the spectrum [54]. Such emission bands have previously been observed in solid-state or dispersed amyloid samples and appear to be associated with the presence of beta-sheet-rich structures formed by aggregation [55].

4.3. Analytical Comparison of AI-Based Methods for Detecting AD Biomarkers

Advances in ML and AI have substantially improved early detection of AD by enabling the identification and quantification of Aβ aggregates and related biomarkers. The reviewed studies apply a range of ML methods across diagnostic platforms — including fluorescence spectroscopy, metabolomics, and blood-based biomarker analysis (see Table 3). Each method presents advantages and challenges, reflecting the diverse potential and current limitations of AI-driven diagnostic strategies in AD research.

Algorithm selection and performance optimization. A key distinction among the reviewed studies lies in the choice of AI/ML methodologies and the nature of the datasets analyzed. Notably, several works highlight the effectiveness of tree-based ensemble learning models—particularly Random Forest (RF) and XGBoost—for handling the complexity and heterogeneity of biological data.

For instance, Han et al. [27] and Karaglani et al. [28] employed these models to classify blood-based biomarkers, achieving impressive AUC values exceeding 0.90, underscoring their robustness and predictive accuracy. Similarly, Li et al. [33] and Du et al. [25] integrated multichannel fluorescence sensor arrays with analytical techniques such as Linear Discriminant Analysis (LDA), Principal Component Analysis (PCA), and RF, achieving classification accuracies greater than 96%. Furthermore, Xu et al. [29] utilized a Multilayer Perceptron (MLP) and RF for miRNA classification in serum and plasma samples, with models surpassing 90% accuracy.

These findings reinforce the suitability of tree-based models, particularly RF and XGBoost, for biomarker detection tasks in AD research, owing to their ability to manage high-dimensional, non-linear, and multivariate biological data effectively.

Feature extraction and dimensionality reduction strategies. Several studies enhanced classification performance by applying statistical decomposition techniques to spectroscopic data. For example, Dos Santos el al. [26] decomposed fluorescence emission spectra into distinct components to identify AD-related spectral variations, applying PARAFAC-QDA and Tucker3-QDA and reaching an accuracy of 94.12%. Similarly, Li et al. [33] and Du et al. [25] employed PCA to reduce the dimensionality of multichannel fluorescence sensor data, facilitating more efficient and accurate classification. In contrast, other studies focused on biological feature extraction, utilizing genomic and metabolic signatures to derive informative features. Han et al., Karaglani et al. and Xu et al. [27–29] exemplify this approach, integrating omics data into their ML models to improve diagnostic accuracy (see Table 3).

Validation methodologies and clinical translation challenges. To ensure analytical robustness, most studies employed cross-validation techniques, and several additionally incorporated independent test sets to validate performance. Han et al. [27] implemented a 10-fold cross-validation approach, achieving an AUC of 0.948 for Alzheimer's diagnosis by integrating metabolic and clinical risk factors. Li et al. [33] reported perfect classification accuracy (100%) in PBS samples, which decreased to 91.7% in serum—highlighting the practical challenges of applying fluorescence-based methods to complex biological matrices. Meanwhile, Karaglani et al. [28] used an AutoML platform (JADBIO) to optimize biomarker selection, achieving an AUC of 0.975 for miRNA-based classification, representing the highest diagnostic performance reported in this review.

Despite the evident potential of AI-based approaches, their widespread application is constrained by limited access to large-scale, high-quality omics datasets, which significantly hinders real-world clinical integration [56]. This scarcity of publicly available data, coupled with the high computational demands of deep learning models, may explain why no such models were identified among the studies reviewed, despite their growing promise in biomedical applications [57]. Nevertheless, Du et al. demonstrated the power

of fluorescence colorimetric sensing combined with hierarchical clustering, achieving 100% classification accuracy in differentiating amyloid fibrils, with high selectivity and sensitivity (LOD: 2.52 nM for insulin fibrils, 14.57 nM for (Aβ) fibrils). Their work highlights the potential of low-cost, smartphone-compatible diagnostic platforms for accessible Alzheimer's screening (see Table 3).

4.4. Limitations

This systematic review adhered strictly to the PRISMA guidelines, employing a rigorous methodology to ensure a comprehensive analysis of existing literature. Despite these efforts, certain limitations must be acknowledged. Firstly, while the search strategy involved multiple reputable databases (Scopus, PubMed, Web of Science, IEEE Xplore) and a well-constructed query string, the possibility of missing relevant studies cannot be entirely ruled out. Some articles may not have been indexed within the selected databases or may have used unconventional terminology, leading to potential gaps in the reviewed literature.

Secondly, a significant limitation arises from the novelty of the research area. Many of the included studies are in preliminary stages. This limitation affects the robustness of the data and the generalizability of the findings, as many studies are yet to undergo the rigorous scrutiny associated with established scientific publications. Additionally, the early developmental status of many diagnostic tools and AI methodologies for AD further constrains the ability to draw definitive conclusions.

Given the emerging nature of ML applications in AD biomarker detection, a key limitation of this review is the lack of availability of standardized, publicly accessible datasets, which currently hinders the feasibility of conducting a comprehensive meta-analysis. The heterogeneity of methods, models, and patient cohorts requires a further qualitative, scoping approach. While this offers valuable insights, it lacks the statistical rigor of meta-analyses and may carry a higher risk of bias. To address this, the review followed PRISMA guidelines, assessing risk of bias by comparing pre-specified outcomes with reported results, and documenting data availability across studies (see Tables 1–3).

Finally, this review identified other broad reviews in related fields, but none of them focused specifically on the research question addressed here. This underscores the originality of this study.

5. Conclusions

5.1. Aβ42/40 Detection in Plasma

Plasma biomarkers are most useful as screening tools to reduce reliance on expensive and invasive PET scans, particularly in research settings and early clinical trials. Plasma Aβ42/40 is a promising non-invasive biomarker for detecting amyloid pathology, with moderate to high accuracy depending on the assay used. However, CSF Aβ42/40 remains the superior predictor of amyloid burden, demonstrating higher sensitivity, specificity, and stronger correlation with amyloid PET.

5.2. Fluorescent Probes

The detection of oligomers is crucial for the early diagnosis of AD. Although many dyes have been studied, most are selective for fibrils rather than oligomers. Only a few of the dyes cited in this work specifically target oligomers [24,34,39,53].

Beyond in vitro binding studies, several ratiometric and NIR probes demonstrate clear advantages over ThT in live models by reducing background fluorescence and improving signal specificity. CRANAD-28, Probe 18, HL_{22} and 2-Me-DABT have been validated for penetration of BBB and in vivo imaging [32,36–38].

5.3. AI for AD Detection

From an AI-analysis perspective, ML methods have demonstrated a strong potential for early AD detection, particularly through the use of tree-based models and statistical techniques for dimensionality reduction. Models like Random Forest and XGBoost performed robustly on various types of biological data, while PCA and LDA helped optimize the classification accuracy. Although deep learning was absent in the reviewed studies, probably due to limited access to large, high-quality omics datasets and computational demands, the overall findings highlight the promise of accessible, cost-effective diagnostic tools, such as smartphone-compatible fluorescence platforms, for future clinical applications.

5.4. Answer to the Primary Research Question

This review directly addresses the three components of the primary question. First, fluorescence-based probes (for example, CRANAD-28, AN-SP and related benzothiazole derivatives) demonstrate sensitive detection of Aβ oligomeric species in vitro and in early ex vivo or small clinical studies, indicating potential to identify aggregate forms that predate fibrillar deposition; however, most probe evidence remains preclinical or derived from small cohorts and therefore requires larger clinical validation. Second, plasma Aβ42/40 consistently decreases in PET-positive individuals (reported reductions $\approx$ 7–18%) and shows assay-dependent discriminative ability (mean AUC $\approx$ 0.80 for mass-spectrometry versus $\approx$0.71 for immunoassays), indicating that the plasma ratio can approximate PET-confirmed amyloid status with reasonable accuracy depending on the assay. Third, AI/ML methods applied to spectral and multivariate plasma data report improved classification in single-study settings and can extract weak multivariate signals; nevertheless, few studies provide independent external validation or direct head-to-head comparisons of *ratio alone* versus *ratio + AI*, so firm conclusions that AI materially increases routine diagnostic performance beyond optimized assays are not yet supported.

5.5. Implications for Clinical Application

Taken together, the evidence suggests different levels of clinical readiness: plasma Aβ42/40—especially when measured by mass spectrometry—currently presents the strongest evidence for identifying PET-confirmed amyloid pathology (AUCs approximately 0.8 in many studies), while fluorescent probes offer a complementary, mechanistic route to detect oligomeric species but mostly remain at proof-of-concept or small clinical scales. AI/ML approaches hold promise to enhance diagnostic algorithms and to combine spectral and fluid markers, but translation into clinical practice will require demonstration of consistent incremental gains in AUC/sensitivity/specificity on external validation cohorts.

5.6. Synthesis and Future Directions

This systematic review shows that plasma Aβ42/40, particularly when measured by mass spectrometry, currently offers the most direct and reproducible approximation to amyloid PET (mean AUC $\approx$ 0.80 in published studies), and therefore represents the most immediately applicable fluid marker for early detection. Fluorescent probes are promising for detecting oligomeric aggregates but remain largely at proof-of-concept or small clinical stages. AI/ML analytical tools can improve signal extraction from complex spectral or multivariate data, but robust evidence of incremental diagnostic benefit (increased AUC, sensitivity, or specificity) over optimized assays is still limited pending externally validated comparisons. Overall, while each approach contributes to early detection in complementary ways, further standardized and externally validated studies are required before routine clinical adoption.

Author Contributions: Conceptualization, S.H., S.M.V.-R., M.N. and W.A.-S.; methodology, S.H. and S.M.V.-R.; formal analysis, S.H.; investigation, S.H. and W.A.-S.; data curation, S.H. and M.N.; writing—original draft preparation, S.H.; writing—review and editing, S.H., S.M.V.-R., M.N. and W.A.-S.; supervision, S.M.V.-R., M.N. and W.A.-S.; All authors have read and agreed to the published version of the manuscript.

Funding: S.H. thanks the Xunta de Galicia for her research scholarship (reference number ED481A and IN606A).

Data Availability Statement: This systematic review was prospectively registered on the Open Science Framework (OSF). The preregistration, including study design, inclusion criteria, and analysis plan, is available at: https://osf.io/4uxeb (accessed on 28 of November 2024) with a registration DOI https://doi.org/10.17605/OSF.IO/4UXEB.

Conflicts of Interest: None of the publications reported conflicts that would compromise the integrity or objectivity of their findings relevant to this review.

References

1. Fandos, N.; Pérez-Grijalba, V.; Pesini, P.; Olmos, S.; Bossa, M.; Villemagne, V.L.; Doecke, J.; Fowler, C.; Masters, C.L.; Sarasa, M.; et al. Plasma amyloid β 42/40 ratios as biomarkers for amyloid β cerebral deposition in cognitively normal individuals. *Alzheimer's Dement. Diagn. Assess. Dis. Monit.* **2017**, *8*, 179–187. [CrossRef]
2. Lansbury, P.T.; Lashuel, H.A. A century-old debate on protein aggregation and neurodegeneration enters the clinic. *Nature* **2006**, *443*, 774–779. [CrossRef]
3. Hardy, J.; Selkoe, D.J. The amyloid hypothesis of Alzheimer's disease: Progress and problems on the road to therapeutics. *Science* **2002**, *297*, 353–356. [CrossRef] [PubMed]
4. Hardy, J.; Bogdanovic, N.; Winblad, B.; Portelius, E.; Andreasen, N.; Cedazo-Minguez, A.; Zetterberg, H. Pathways to Alzheimer's disease. *J. Intern. Med.* **2014**, *275*, 296–303. [CrossRef] [PubMed]
5. Kepp, K.P.; Robakis, N.K.; Høilund-Carlsen, P.F.; Sensi, S.L.; Vissel, B. The amyloid cascade hypothesis: An updated critical review. *Brain* **2023**, *146*, 3969–3990. [CrossRef]
6. Long, J.M.; Holtzman, D.M. Alzheimer Disease: An Update on Pathobiology and Treatment Strategies. *Cell* **2019**, *179*, 312–339. [CrossRef]
7. Bilgel, M.; An, Y.; Walker, K.A.; Moghekar, A.R.; Ashton, N.J.; Kac, P.R.; Karikari, T.K.; Blennow, K.; Zetterberg, H.; Jedynak, B.M.; et al. Longitudinal changes in Alzheimer's-related plasma biomarkers and brain amyloid. *Alzheimer's Dement. J. Alzheimer's Assoc.* **2023**, *19*, 4335–4345. [CrossRef]
8. Lee, S.J.C.; Nam, E.; Lee, H.J.; Savelieff, M.G.; Lim, M.H. Towards an understanding of amyloid-β oligomers: Characterization, toxicity mechanisms, and inhibitors. *Chem. Soc. Rev.* **2017**, *46*, 310–323. [CrossRef]
9. Hampel, H.; Hardy, J.; Blennow, K.; Chen, C.; Perry, G.; Kim, S.H.; Villemagne, V.L.; Aisen, P.; Vendruscolo, M.; Iwatsubo, T.; et al. The Amyloid-β Pathway in Alzheimer's Disease. *Mol. Psychiatry* **2021**, *26*, 5481–5503. [CrossRef]
10. Viola, K.L.; Bicca, M.A.; Bebenek, A.M.; Kranz, D.L.; Nandwana, V.; Waters, E.A.; Haney, C.R.; Lee, M.; Gupta, A.; Brahmbhatt, Z.; et al. The Therapeutic and Diagnostic Potential of Amyloid β Oligomers Selective Antibodies to Treat Alzheimer's Disease. *Front. Neurosci.* **2022**, *15*, 768646. [CrossRef]
11. Cline, E.N.; Bicca, M.A.; Viola, K.L.; Klein, W.L.; Perry, G.; Avila, J.; Moreira, P.; Sorensen, A.; Tabaton, M. The Amyloid-β Oligomer Hypothesis: Beginning of the Third Decade. *J. Alzheimer's Dis.* **2018**, *64*, S567–S610. [CrossRef] [PubMed]
12. Allué, J.A.; Pascual-Lucas, M.; Sarasa, L.; Castillo, S.; Sarasa, M.; Sáez, M.E.; Abdel-Latif, S.; Rissman, R.A.; Terencio, J. Clinical utility of an antibody-free LC-MS method to detect brain amyloid deposition in cognitively unimpaired individuals from the screening visit of the A4 Study. *Alzheimer's Dement. Diagn. Assess. Dis. Monit.* **2023**, *15*, e12451. [CrossRef] [PubMed]
13. Pascual-Lucas, M.; Allué, J.A.; Sarasa, L.; Fandos, N.; Castillo, S.; Terencio, J.; Sarasa, M.; Tartari, J.P.; Sanabria, Á.; Tárraga, L.; et al. Clinical performance of an antibody-free assay for plasma Aβ42/Aβ40 to detect early alterations of Alzheimer's disease in individuals with subjective cognitive decline. *Alzheimer's Res. Ther.* **2023**, *15*, 2. [CrossRef]
14. Udeh-Momoh, C.; Zheng, B.; Sandebring-Matton, A.; Novak, G.; Kivipelto, M.; Jönsson, L.; Middleton, L. Blood Derived Amyloid Biomarkers for Alzheimer's Disease Prevention. *J. Prev. Alzheimer's Dis.* **2022**, *9*, 12–21. [CrossRef]
15. Gao, F.; Lv, X.; Dai, L.; Wang, Q.; Wang, P.; Cheng, Z.; Xie, Q.; Ni, M.; Wu, Y.; Chai, X.; et al. A combination model of AD biomarkers revealed by machine learning precisely predicts Alzheimer's dementia: China Aging and Neurodegenerative Initiative (CANDI) study. *Alzheimer's Dement. J. Alzheimer's Assoc.* **2022**, *19*, 749–760. [CrossRef]

16. Weber, D.M.; Taylor, S.W.; Lagier, R.J.; Kim, J.C.; Goldman, S.M.; Clarke, N.J.; Vaillancourt, D.E.; Duara, R.; McFarland, K.N.; Wang, W.E.; et al. Clinical utility of plasma Aβ42/40 ratio by LC-MS/MS in Alzheimer's disease assessment. *Front. Neurol.* **2024**, *15*, 1364658. [CrossRef]
17. Meyer, M.R.; Kirmess, K.M.; Eastwood, S.; Wente-Roth, T.; Irvin, F.; Holubasch, M.S.; Venkatesh, V.; Fogelman, I.; Monane, M.; Hanna, L.; et al. Clinical validation of the PrecivityAD2 blood test: A mass spectrometry-based test with algorithm combining %p-tau217 and Aβ42/40 ratio to identify presence of brain amyloid. *Alzheimer's Dement.* **2024**, *20*, 3179–3192. [CrossRef]
18. Zicha, S.; Bateman, R.J.; Shaw, L.M.; Zetterberg, H.; Bannon, A.W.; Horton, W.A.; Baratta, M.; Kolb, H.C.; Dobler, I.; Mordashova, Y.; et al. Comparative analytical performance of multiple plasma Aβ42 and Aβ40 assays and their ability to predict positron emission tomography amyloid positivity. *Alzheimer's Dement. J. Alzheimer's Assoc.* **2022**, *19*, 956–966. [CrossRef]
19. Schindler, S.E.; Bollinger, J.G.; Ovod, V.; Mawuenyega, K.G.; Li, Y.; Gordon, B.A.; Holtzman, D.M.; Morris, J.C.; Benzinger, T.L.S.; Xiong, C.; et al. High-precision plasma β-amyloid 42/40 predicts current and future brain amyloidosis. *Neurology* **2019**, *93*, E1647–E1659. [CrossRef]
20. Wisch, J.K.; Gordon, B.A.; Boerwinkle, A.H.; Luckett, P.H.; Bollinger, J.G.; Ovod, V.; Li, Y.; Henson, R.L.; West, T.; Meyer, M.R.; et al. Predicting continuous amyloid PET values with CSF and plasma Aβ42/Aβ40. *Alzheimer's Dement.* **2023**, *15*, e12405. [CrossRef]
21. Li, Y.; Schindler, S.E.; Bollinger, J.G.; Ovod, V.; Mawuenyega, K.G.; Weiner, M.W.; Shaw, L.M.; Masters, C.L.; Fowler, C.J.; Trojanowski, J.Q.; et al. Validation of Plasma Amyloid-β 42/40 for Detecting Alzheimer Disease Amyloid Plaques. *Neurology* **2022**, *98*, E688–E699. [CrossRef]
22. West, T.; Kirmess, K.M.; Meyer, M.R.; Holubasch, M.S.; Knapik, S.S.; Hu, Y.; Contois, J.H.; Jackson, E.N.; Harpstrite, S.E.; Bateman, R.J.; et al. A blood-based diagnostic test incorporating plasma Aβ42/40 ratio, ApoE proteotype, and age accurately identifies brain amyloid status: Findings from a multi cohort validity analysis. *Mol. Neurodegener.* **2021**, *16*, 30. [CrossRef]
23. Aliyan, A.; Cook, N.P.; Martí, A.A. Interrogating Amyloid Aggregates using Fluorescent Probes. *Chem. Rev.* **2019**, *119*, 11819–11856. [CrossRef]
24. Li, C.; Yang, L.; Han, Y.; Wang, X. A simple approach to quantitative determination of soluble amyloid-β peptides using a ratiometric fluorescence probe. *Biosens. Bioelectron.* **2019**, *142*, 111518. [CrossRef]
25. Du, J.Q.; Luo, W.C.; Zhang, J.T.; Li, Q.Y.; Bao, L.N.; Jiang, M.; Yu, X.; Xu, L. Machine learning-assisted fluorescence/fluorescence colorimetric sensor array for discriminating amyloid fibrils. *Sens. Actuators B-Chem.* **2024**, *417*, 136173. [CrossRef]
26. Dos Santos, R.F.; Paraskevaidi, M.; Mann, D.M.A.; Allsop, D.; Santos, M.C.D.; Morais, C.L.M.; Lima, K.M.G. Alzheimer's disease diagnosis by blood plasma molecular fluorescence spectroscopy (EEM). *Sci. Rep.* **2022**, *12*, 16199. [CrossRef] [PubMed]
27. Han, L.Y.; Chen, X.; Wang, Y.; Zhang, R.J.; Zhao, T.; Pu, L.Y.; Huang, Y.; Sun, H.P. A machine learning algorithm based on circulating metabolic biomarkers offers improved predictions of neurological diseases. *Clin. Chim. Acta* **2024**, *558*, 119671. [CrossRef]
28. Karaglani, M.; Gourlia, K.; Tsamardinos, I.; Chatzaki, E. Accurate Blood-Based Diagnostic Biosignatures for Alzheimer's Disease via Automated Machine Learning. *J. Clin. Med.* **2020**, *9*, 3016. [CrossRef]
29. Xu, A.; Kouznetsova, V.L.; Tsigelny, I.F. Alzheimer's Disease Diagnostics Using miRNA Biomarkers and Machine Learning. *J. Alzheimer's Dis. JAD* **2022**, *86*, 841–859. [CrossRef]
30. Klunk, W.E.; Koeppe, R.A.; Price, J.C.; Benzinger, T.L.; Devous, M.D.; Jagust, W.J.; Johnson, K.A.; Mathis, C.A.; Minhas, D.; Pontecorvo, M.J.; et al. The Centiloid Project: Standardizing quantitative amyloid plaque estimation by PET. *Alzheimer's Dement.* **2015**, *11*, 1–15. [CrossRef]
31. Banack, S.A.; Stark, A.C.; Cox, P.A. A possible blood plasma biomarker for early-stage Alzheimer's disease. *PLoS ONE* **2022**, *17*, e0267407. [CrossRef]
32. Telpoukhovskaia, M.A.; Cawthray, J.F.; Rodríguez-Rodríguez, C.; Scott, L.E.; Page, B.D.G.; Patrick, B.O.; Orvig, C. 3-Hydroxy-4-pyridinone derivatives designed for fluorescence studies to determine interaction with amyloid protein as well as cell permeability. *Bioorg. Med. Chem. Lett.* **2015**, *25*, 3654–3657. [CrossRef]
33. Li, F.; Zhou, L.; Gao, X.; Ni, W.; Hu, J.; Wu, M.; Chen, S.; Han, J.; Wu, J. A Multichannel Fluorescent Tongue for Amyloid-β Aggregates Detection. *Int. J. Mol. Sci.* **2022**, *23*, 14562. [CrossRef] [PubMed]
34. Lv, G.; Sun, A.; Wei, P.; Zhang, N.; Lan, H.; Yi, T. A spiropyran-based fluorescent probe for the specific detection of β-amyloid peptide oligomers in Alzheimer's disease. *Chem. Commun.* **2016**, *52*, 8865–8868. [CrossRef] [PubMed]
35. Nabers, A.; Ollesch, J.; Schartner, J.; Kötting, C.; Genius, J.; Hafermann, H.; Klafki, H.; Gerwert, K.; Wiltfang, J. Amyloid-β-Secondary Structure Distribution in Cerebrospinal Fluid and Blood Measured by an Immuno-Infrared-Sensor: A Biomarker Candidate for Alzheimer's Disease. *Anal. Chem.* **2016**, *88*, 2755–2762. [CrossRef]
36. Mora, A.K.; Murudkar, S.; Alamelu, A.; Singh, P.K.; Chattopadhyay, S.; Nath, S. Benzothiazole-Based Neutral Ratiometric Fluorescence Sensor for Amyloid Fibrils. *Chemistry* **2016**, *22*, 16505–16512. [CrossRef]
37. Ran, K.; Yang, J.; Nair, A.V.; Zhu, B.; Ran, C. CRANAD-28: A Robust Fluorescent Compound for Visualization of Amyloid Beta Plaques. *Molecules* **2020**, *25*, 863. [CrossRef]

38. Zhou, K.; Yuan, C.; Dai, B.; Wang, K.; Chen, Y.; Ma, D.; Dai, J.; Liang, Y.; Tan, H.; Cui, M. Environment-Sensitive Near-Infrared Probe for Fluorescent Discrimination of Aβ and Tau Fibrils in AD Brain. *J. Med. Chem.* **2019**, *62*, 6694–6704. [CrossRef]
39. Chen, C.H.; Jong, Y.J.; Chao, Y.Y.; Wang, C.C.; Chen, Y.L. Fluorescent aptasensor based on conformational switch-induced hybridization for facile detection of β-amyloid oligomers. *Anal. Bioanal. Chem.* **2022**, *414*, 8155–8165. [CrossRef]
40. Freire, S.; De Araujo, M.H.; Al-Soufi, W.; Novo, M. Photophysical study of Thioflavin T as fluorescence marker of amyloid fibrils. *Dye. Pigment.* **2014**, *110*, 97–105. [CrossRef]
41. Xue, C.; Lin, T.Y.; Chang, D.; Guo, Z. Thioflavin T as an amyloid dye: Fibril quantification, optimal concentration and effect on aggregation. *R. Soc. Open Sci.* **2017**, *4*, 160696. [CrossRef] [PubMed]
42. National Institute on Aging. Alzheimer's Disease Genetics Fact Sheet. 2023. Available online: https://www.nia.nih.gov/health/alzheimers-causes-and-risk-factors/alzheimers-disease-genetics-fact-sheet (accessed on 15 April 2025).
43. Petit, D.; Fernández, S.G.; Zoltowska, K.M.; Enzlein, T.; Ryan, N.S.; O'Connor, A.; Szaruga, M.; Hill, E.; Vandenberghe, R.; Fox, N.C.; et al. Aβ profiles generated by Alzheimer's disease causing PSEN1 variants determine the pathogenicity of the mutation and predict age at disease onset. *Mol. Psychiatry* **2022**, *27*, 2821–2832. [CrossRef] [PubMed]
44. Potter, R.R., III; Long, A.P.; Lichtenstein, M.L. Population prevalence of autosomal dominant Alzheimer's disease: A systematic review. *Alzheimer's Dement.* **2020**, *16*, e037129. [CrossRef]
45. Yuyama, K.; Sun, H.; Mitsutake, S.; Igarashi, Y. Sphingolipid-modulated exosome secretion promotes clearance of amyloid-β by microglia. *J. Biol. Chem.* **2012**, *287*, 10977–10989. [CrossRef]
46. Sardar Sinha, M.; Ansell-Schultz, A.; Civitelli, L.; Hildesjö, C.; Larsson, M.; Lannfelt, L.; Ingelsson, M.; Hallbeck, M. Alzheimer's disease pathology propagation by exosomes containing toxic amyloid-beta oligomers. *Acta Neuropathol.* **2018**, *136*, 41–56. [CrossRef]
47. Ovod, V.; Ramsey, K.N.; Mawuenyega, K.G.; Bollinger, J.G.; Hicks, T.; Schneider, T.; Sullivan, M.; Paumier, K.; Holtzman, D.M.; Morris, J.C.; et al. Amyloid β concentrations and stable isotope labeling kinetics of human plasma specific to central nervous system amyloidosis. *Alzheimer's Dement. J. Alzheimer's Assoc.* **2017**, *13*, 841–849. [CrossRef]
48. Delaby, C.; Estellés, T.; Zhu, N.; Arranz, J.; Barroeta, I.; Carmona-Iragui, M.; Illán-Gala, I.; Santos-Santos, M.Á.; Altuna, M.; Sala, I.; et al. The Aβ1–42/Aβ1–40 ratio in CSF is more strongly associated to tau markers and clinical progression than Aβ1–42 alone. *Alzheimer's Res. Ther.* **2022**, *14*, 20. [CrossRef]
49. Janelidze, S.; Palmqvist, S.; Leuzy, A.; Stomrud, E.; Verberk, I.M.W.; Zetterberg, H.; Ashton, N.J.; Pesini, P.; Sarasa, L.; Allué, J.A.; et al. Detecting amyloid positivity in early Alzheimer's disease using combinations of plasma Aβ42/Aβ40 and p-tau. *Alzheimer's Dement.* **2022**, *18*, 283–293. [CrossRef]
50. Ashton, N.J.; Janelidze, S.; Mattsson-Carlgren, N.; Binette, A.P.; Strandberg, O.; Brum, W.S.; Karikari, T.K.; González-Ortiz, F.; Di Molfetta, G.; Meda, F.J.; et al. Differential roles of Aβ42/40, p-tau231 and p-tau217 for Alzheimer's trial selection and disease monitoring. *Nat. Med.* **2022**, *28*, 2555–2562. [CrossRef]
51. Ingannato, A.; Bagnoli, S.; Mazzeo, S.; Giacomucci, G.; Bessi, V.; Ferrari, C.; Sorbi, S.; Nacmias, B. Plasma GFAP, NfL and pTau 181 detect preclinical stages of dementia. *Front. Endocrinol.* **2024**, *15*, 1375302. [CrossRef]
52. Chatterjee, P.; Pedrini, S.; Stoops, E.; Goozee, K.; Villemagne, V.L.; Asih, P.R.; Verberk, I.M.W.; Dave, P.; Taddei, K.; Sohrabi, H.R.; et al. Plasma glial fibrillary acidic protein is elevated in cognitively normal older adults at risk of Alzheimer's disease. *Transl. Psychiatry* **2021**, *11*, 27. [CrossRef]
53. Li, Y.; Xu, D.; Sun, A.; Ho, S.L.; Poon, C.Y.; Chan, H.N.; Ng, O.T.W.; Yung, K.K.L.; Yan, H.; Li, H.W.; et al. Fluoro-substituted cyanine for reliable in vivo labelling of amyloid-β oligomers and neuroprotection against amyloid-β induced toxicity. *Chem. Sci.* **2017**, *8*, 8279–8284. [CrossRef]
54. Novo, M.; Illodo, S.; Seijas, J.; Hernández, S.; Rodríguez-Prieto, F.; Al-Soufi, W. Intrinsic visible emission of amyloid-β oligomers: A potential tool for early alzheimer's diagnosis. *Phys. Chem. Chem. Phys.* **2025**, *27*, 16733–16737. [CrossRef]
55. Balasco, N.; Diaferia, C.; Rosa, E.; Monti, A.; Ruvo, M.; Doti, N.; Vitagliano, L. A Comprehensive Analysis of the Intrinsic Visible Fluorescence Emitted by Peptide/Protein Amyloid-like Assemblies. *Int. J. Mol. Sci.* **2023**, *24*, 8372. [CrossRef]
56. Tran, K.A.; Kondrashova, O.; Bradley, A.; Williams, E.D.; Pearson, J.V.; Waddell, N. Deep learning in cancer diagnosis, prognosis and treatment selection. *Genome Med.* **2021**, *13*, 152. [CrossRef]
57. Alzubaidi, A.; Tepper, J.; Lotfi, A. A novel deep mining model for effective knowledge discovery from omics data. *Artif. Intell. Med.* **2020**, *104*, 101821. [CrossRef]